Natural Hazards
and Earth System
Sciences
Discussions

A cross-scale study for compound flooding processes during Hurricane Florence

Fei Ye[1], Wei Huang[1], Yinglong J. Zhang[1], Saeed Moghimi[2], Edward Myers[2], Shachak Pe'eri[2], Hao-Cheng Yu[1]

[1]Virginia Institute of Marine Science, College of William & Mary, Gloucester Point, 23062, USA

5   [2] NOAA National Ocean Service, Silver Spring, 20910, USA

Correspondence to: Fei Ye (feiye@vims.edu)

Abstract

We study the compound flooding processes as occurred in Hurricane Florence (2018) that was accompanied by heavy precipitation, using a 3D creek-to-ocean hydrodynamic model. We examine the important role played by barrier islands in

10   the observed compound surges in the coastal watershed. Locally very high resolution is used in some watershed areas in order to resolve small features that turn out to be critical for capturing the observed High Water Marks locally. The wave effects are found to be significant near barrier islands and have contributed to some observed over-toppings and breaches. Sensitivity results from applying each of the three major forcing factors (oceanic, fluvial and pluvial) *separately* are succinctly summarized in a "dominance map" that highlights significant compound effects in most of the affected coastal

15   watersheds, estuaries and back bays behind the barrier islands. Operational forecasts based on the current model are being set up at NOAA to help coastal resource and emergency managers with disaster planning and mitigation effort.

1 Introduction

Recently, more frequent occurrences of "wet" hurricanes (i.e. hurricanes accompanied by heavy precipitation) that stall

20   near the coast (Pfahl et al., 2017; Hall and Kossin, 2019) have brought new challenges to coastal communities in the form of compound flooding, which is defined as concurrence of flooding from same or different origins (river, storm surge and rainfall), especially in the coastal transitional zone that sits at the border between coastal, estuarine, and hydrologic regimes (Santiago-Collazo et al., 2019). Compound flooding highlights one of the major pitfalls of the current hurricane intensity scale, which is entirely based on wind speed, leaving the potential rainfall and flooding impacts to be glossed over in initial

25   forecasts that emphasize hurricane category. The record-setting 2020 Atlantic hurricane season including a number of very wet storms highlights the urgency, and exposes the current knowledge gap, for understanding compound flooding processes.

A recent example for compound flood events is Hurricane Florence that impacted a large area of North Carolina (NC) in September 2018. Hurricane Florence was the first major hurricane of the 2018 Atlantic hurricane season. Originated from a

strong tropical wave near Cape Verde, west Africa, it acquired tropical storm strength on September 1, followed by a rapid
30   intensification to a Category 4 status on September 4, with estimated maximum sustained winds of 130 mph, and eventually
reached its maximum strength on September 11. It made landfall south of Wrightsville Beach, near the border between NC
and South Carolina (SC) as a Category 1 hurricane on September 14. The slow motion of the storm after the landfall brought
heavy rainfall throughout the Carolinas for several days. Compounded by the storm surge, the rainfall caused widespread
flooding along a large swath of the NC coast, and inland flooding from Florence inundated cities such as Fayetteville,
35   Smithfield, Lumberton, Durham, and Chapel Hill. According to USGS report (Fester et al., 2018), a new record rainfall total
of 35.93 inches was set during the hurricane in Elizabethtown, NC. Many other locations throughout NC and SC also set
new records for rainfall (Fig. 1). Florence is a quintessential example of major flooding that a slow moving, moisture-laden
storm can bring, even if it does not have strong hurricane wind.

In this paper, we will study the response to the storm in the watershed rivers and estuaries and examine the processes and
40   sources that lead to the compound flooding there. We will also examine the coastal responses to the event and the close
connection between watershed and coastal ocean. The existing modeling efforts on compound flooding (Chen et al., 2010;
Cho et al., 2012; Dresback et al., 2013; Chen and Liu, 2014; Ikeuchi et al., 2017; Kumbier et al., 2018; Pasquier et al., 2018;
Wing et al., 2019; Muñoz et al., 2020) often focus on a subset of the processes (storm surges, tides, waves, fluvial flooding,
pluvial flooding, and potential baroclinic effects), leaving gaps in accurately representing the complex interactions among
45   them (Santiago-Collazo et al., 2019). What distinguishes this study from traditional compound flooding simulations is a
holistic approach that includes interrelated processes in different regimes and on multiple temporal/spatial scales in a single
modeling framework. An overview of the processes studied in this paper is shown in Fig. 2. The primary tool used in this
study is a proven cross-scale 3D baroclinic model designed for effective and holistic simulation of intertwined processes as
found during this event. We chose a 3D model instead of a more efficient 2D model because as demonstrated in Ye et al.
50   (2020), large-scale processes (e.g. Gulf Stream) can affect the total water level through the process of baroclinic adjustment
especially after the storm; specifically, a 3D baroclinic model can lead to better predictions of sub-tidal elevations that are
important for the inundation process. In addition, a 3D model can also produce relevant 3D variables (velocity, tracers etc)
that are important for safe navigation and ecosystem health. The 3D model presented in this paper is efficient enough for
operational forecasts, which are being set up at NOAA (National Oceanic and Atmospheric Administration).

55   The paper is structured as follows. Section 2 will review the study site and available observations collected during the event
in the watershed, estuaries, and coastal ocean. Section 3 describes the numerical model used and its set-up including its
coupling to National Water Model version 2.0 (NWM; the hydrological model that provides the river flows). Section 4
presents model validation and important sensitivity test results; the validation is done in a cross-scale fashion from small-
scale watershed areas to large-scale coastal ocean. Section 5 discusses the compound effects as revealed by the 3D model in
60   all regimes. Section 6 summarizes the major findings of the paper and planned follow-up work.
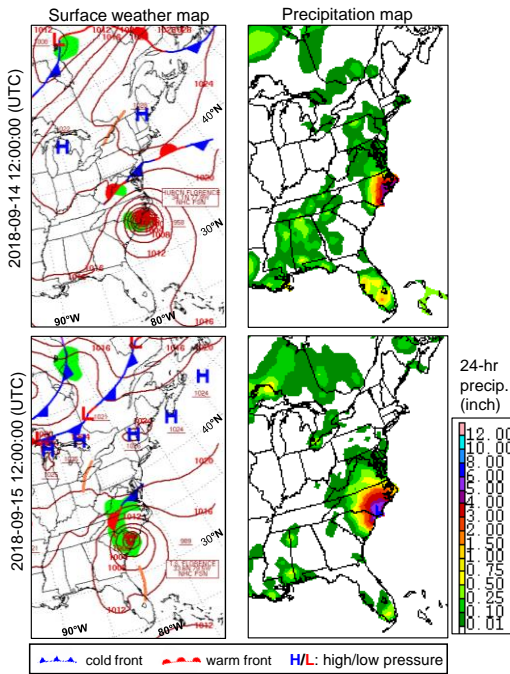
Fig. 1: Weather map showing the low-pressure system and amount of rainfall Florence brought to NC and SC coast around landfall. Credit: NOAA Central Library U.S. Daily Weather Maps Project (https://www.wpc.ncep.noaa.gov/dailywxmap/explaination.html); partial views of the original online maps.
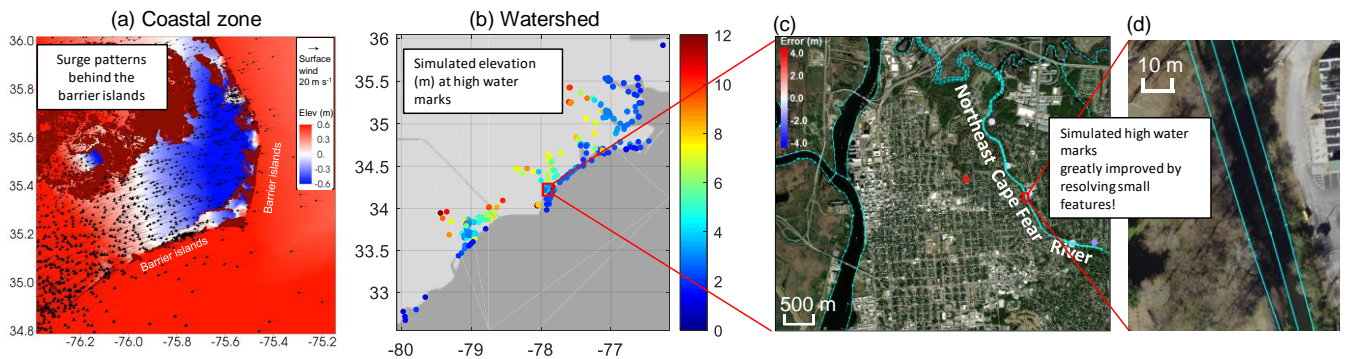
65

Fig. 2: Overview of the processes studied in the paper, from (a) coastal zone to (b) watershed, and down to very small local scales in the watershed in (c) and (d). The base maps in (c) and (d) are provided by ESRI.

70 **2 Study site and observation**

The focus (high-resolution) area of this study is on the NC and SC coast and coastal watersheds that saw most of the impact from Florence (Fig. 3b and Fig. 3f). Similar to what we did for other hurricane events, the domain landward boundary is set at 10 m above sea level, which is deemed sufficient to capture most backwater effects (Ye et al., 2020; Zhang et al., 2020). A

3

rich set of observations for physical and biological variables are available from satellites, autonomous instruments (e.g.

75   gliders, Argo floats), in situ stations operated by NOAA and USGS's field estimates collected during after-event surveys (e.g. High Water Marks (HWMs)) (Fig. 2b and Fig. 2c). Analysis and quality control of these datasets have been done by the data distributors, together with uncertainty assessments. Some of the datasets will be presented in the context of model validation sections below to allow for a comprehensive and objective assessment of the model errors and uncertainties. Assessment of compound flood models such as ours inevitably involves observation collected at disparate spatial and

80   temporal scales of several orders of magnitudes contrasts, as illustrated in Fig. 2. To the best of our knowledge, this type of model assessment has rarely been attempted before even in 2D setting, due to the formidable challenges to numerical models (Santiago-Collazo et al., 2019), but is badly needed in order to gain a holistic understanding of the complex processes at play (Ye et al., 2020; Zhang et al., 2020; Huang et al., submitted).
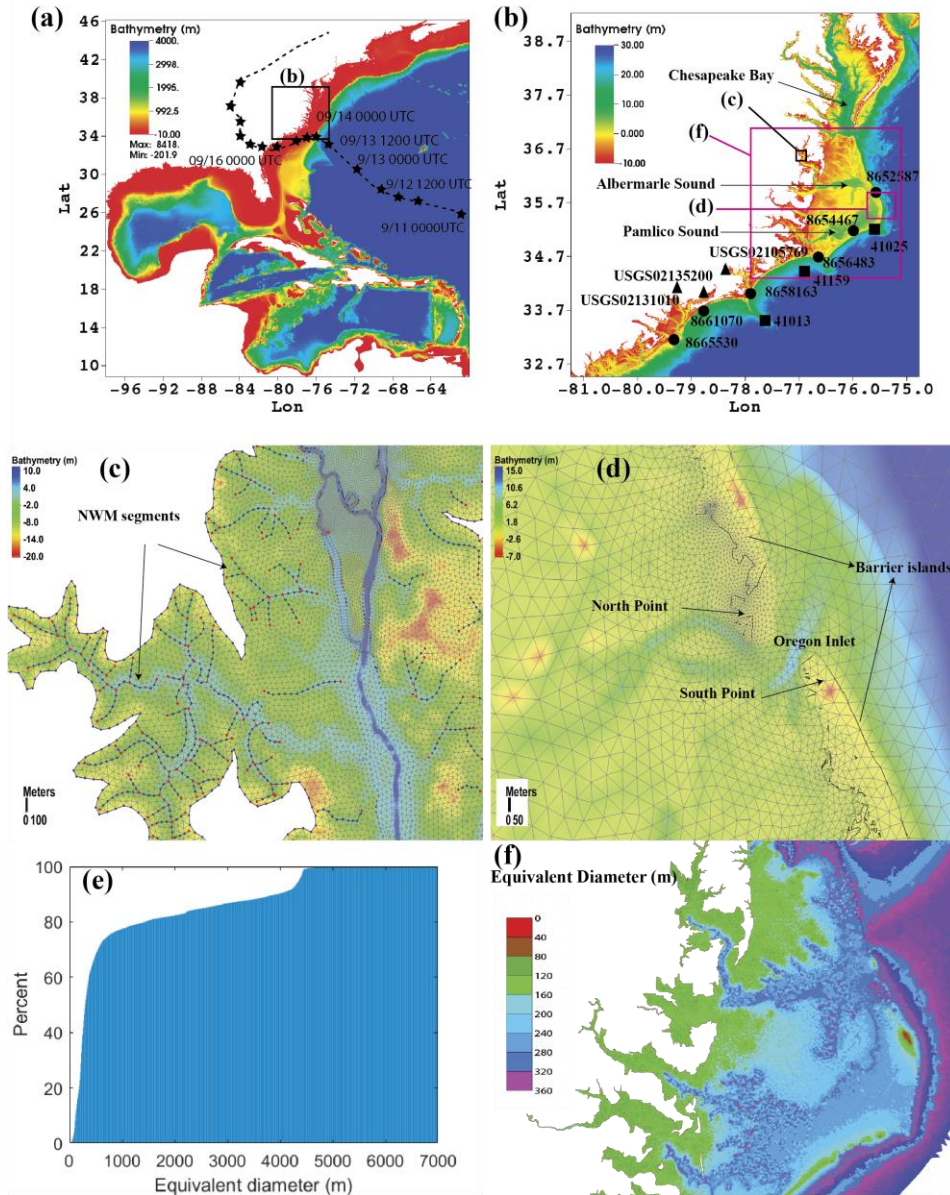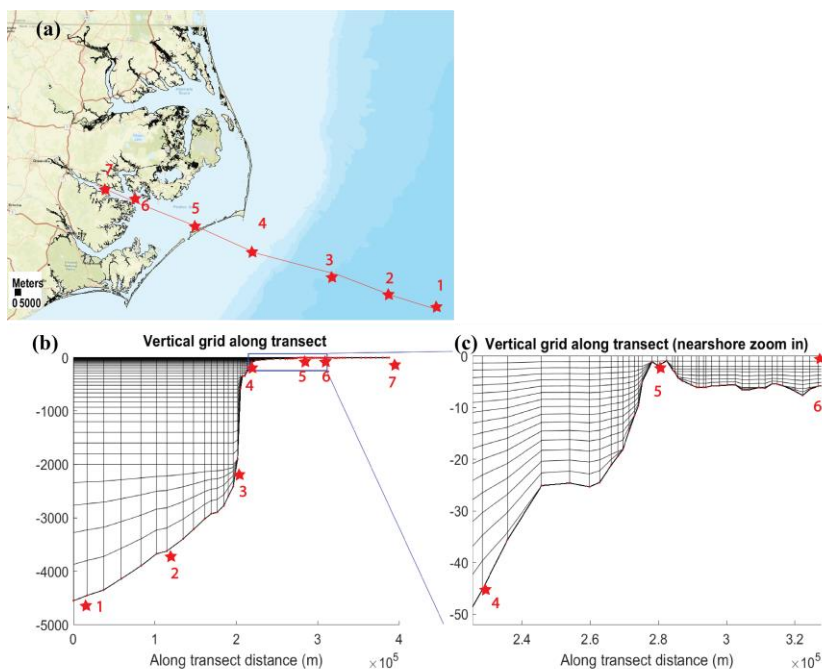
Fig. 3: Model domain and horizontal grid. (a) Domain extent and hurricane track. (b) Station locations along the North Carolina and South Carolina coast. The six NOAA gauges are: Charleston (8665530); Springmaid Pier (8661070); Wrightsville Beach (8658163); Beaufort (8656483); Hatteras (8654467); Oregon Inlet (8652587). The 3 squares are NDBC buoys (41013, 41159, 41025). The spatial extents of (c), (d), and (f) are also marked in (b). (c) Zoom-in of grid in a watershed area (the arcs are from NWM river network). (d) Zoom-in of grid near barrier islands and inlet (the dark line is the 0 m isobath); (e) Cumulative histogram of grid resolution (measured in equivalent diameters); (f) Grid resolution in North Carolina's coastal watershed area.

85

90

Fig. 4: Vertical grid. (a) Transect from coastal ocean into watershed, used to show the vertical grid; (b) vertical grid along the transect; (c) zoom-in from (b), illustrating the transitions from 3D (in coastal ocean) to 2DH (on barrier island) and back to 3D (back bay).

3 Model description

3.1 Model setups

To capture the storm surge effects we use a large study domain that encompasses the north Atlantic west of 60°W (Fig. 3a). An added benefit of using such a large domain in conjunction of a 3D baroclinic model is that the interaction between large- and small-scale processes can be organically examined in a single model; as explained by Ye et al. (2020), the disruption and oscillation of Gulf Stream by storms can directly affect the coastal inundation (i.e. fair-weather flooding described by Ezer 2018). Our results suggest that the converse is also true, as watershed processes can also affect Gulf Stream and other coastal processes. Therefore, a seamless creek-to-ocean model is advantageous for compound flood studies.

As one of the first bona fide compound surge and flood models, SCHISM (schism.wiki; Zhang et al., 2016) uses a very efficient semi-implicit solver to solve the hydrostatic form of the Navier-Stokes equations. Major characteristics of the model that ensure a balance of accuracy, efficiency, robustness and flexibility include: hybrid finite-element/finite-volume methods and a highly flexible 3D gridding system ("polymorphism") that combines a hybrid triangular-quadrangular unstructured grid in the horizontal dimension and a hybrid LSC^2 grid in the vertical (Zhang et al., 2015). The polymorphism allows a single SCHISM grid to seamlessly morph between full 3D, 2DH (2D depth-averaged), 2DV (2D laterally averaged), and quasi-1D configurations. The employment of shaved cells near the bottom in particular faithfully preserves the original

bathymetry without any smoothing required. The detrimental effects of bathymetry smoothing on important physical and biological processes (e.g. residual transport, lateral circulation, nutrient cycling etc) have been carefully documented in Ye et

115 al. (2018) and Cai et al. (2020).

Similar to a recent compound flooding study using SCHISM for Hurricane Harvey (Huang et al., submitted), the current model domain covers the entire US East Coast and the entire Gulf of Mexico, with all major bays/estuaries and coastal watersheds resolved (Fig. 3). The horizontal grid, generated using the software SMS (aquaveo.com), has 2.2 million nodes and 4.4 million elements (Fig. 3). About 50% and 40% of the elements have resolution finer than 300m and 220m

120 respectively (Fig. 3e). Land boundary is located at 10 m above sea level. The grid bathymetry is interpolated from a combination of DEM sources from coarse (ETOPO1, 90m Coastal Relief Model (https://ngdc.noaa.gov/mgg/coastal/crm.html)) to fine resolution (1/9 arc-second CUDEM (https://www.ncei.noaa.gov/metadata/geoportal/rest/metadata/item/gov.noaa.ngdc.mgg.dem:999919/html), 1−3 m CoNED (https://www.usgs.gov/core-science-systems/eros/coned)), and the vertical datum used is NAVD88, with appropriate

125 conversion between datums done by VDatum tool (vdatum.noaa.gov). Altogether close to 400 DEM tiles are used to cover such a large region. Note that NAVD88 is a more convenient datum to use in the model as most of recent observation data refer to this datum, and therefore we use this datum in the model setup and allow the model to automatically set up the sub-tidal surface slope from coastal ocean into watershed (due to the friction effects). The horizontal grid resolution ranges from 6−7 km in the open ocean to ~400 m near the shoreline, with barrier island and narrow inlets resolved; river channels and

130 creeks represented by NWM streams have about 300 m along-channel resolution and variable cross-channel resolutions to ensure adequate representation of the channelized flow. Shipping channels are represented by quadrangles and have 20 m or finer cross-channel resolution in NC. The finest grid resolution used is ~1 m used to represent many levees in other parts of the coast; note that as an implicit model SCHISM has no CFL constraint and thus can handle high resolution efficiently. Watershed region of the grid has explicitly incorporated close to 300K NWM segments ("thalwegs"; cf. Fig. 3c), to facilitate

135 the routing of river flow and precipitated water there. Customary of all SCHISM applications, no manipulation or smoothing of bathymetry was done in the computational grid after interpolation of the depths from DEMs (including steep slopes in the Caribbean and all shipping channels). In the vertical dimension we use 1−43 layers, with 43 layers being applied in the deep ocean and 1 layer in most of the watershed (Fig. 4), thus effectively rendering the model 2DH there, which is sufficient for flow routing and inundation processes.

140 Table 1 shows the setups for "baseline" and a few important sensitivity simulations used in this paper. For the baseline, imposed at the ocean boundary (60°W) are tidal elevation and barotropic velocity of 8 tidal constituents (S2, M2, N2, K2, K1, P1, O1, and Q1), extracted from the FES2014 database (https://datastore.cls.fr/catalogues/fes2014-tide-model/). The baroclinic components for the elevation and velocity are derived from the daily HYCOM outputs. The initial condition for the water elevation is set to be 0 in all areas with positive depths ("wet") and to be equal to the bottom elevation at "dry"

145 watershed locations (so that the total water depth there is equal to 0 initially). The initial condition for the horizonal velocity is zero in the watershed and is interpolated from HYCOM elsewhere. Commensurate with the non-zero velocity (fully

dynamic state) are salinity and temperature values interpolated from HYCOM; however, in the nearshore areas where HYCOM results are less accurate, the initial conditions for salinity and temperature are interpolated from the sparse observation at several USGS gauges in order to speed up the dynamic adjustment process. The surface meteorological
150 forcing applied in the model is a combination of two products: (1) a high-resolution ERA re-analysis product from the European Centre for Medium-range Weather Forecast (ECMWF) with a ~9 km horizontal resolution (cf. Acknowledgements), and (2) a 3 h time interval with NOAA's High-Resolution Rapid Refresh (HRRR; https://rapidrefresh.noaa.gov/hrrr/), which is a cloud-resolving and convection-allowing atmospheric model with a 3 km horizontal resolution and a 1 h time interval. Bottom friction coefficient is set at a constant value of 0.0025 at all "wet"
155 locations, then linearly increases to 0.025 as the ground elevation increases from 1 m to 3 m (above NAVD88). A constant value of 0.025 is used for higher grounds where the bed texture is generally rougher than the riverbed (Ye et al., 2020). The tuning of friction values is intentionally kept to minimum in favour of simplicity and ease of extension to national scale, while leaving room for fine adjustment if the information on sediment characteristics and bedforms is available in a specific system in the future. The method used to impose the river flow in the model is described in the next subsection.

160 Choices of the "baseline" model parameters are similar to those used for Irene (Ye et al., 2020). The time step is 150 seconds (sensitivity tests using 100−150 s gave very similar results). The level-2.5 equation turbulence closure scheme chosen is from the generic length scale model of *k-kl* (Umlauf and Burchard, 2003). The simulation starts from 2018-08-24 00:00 (UTC) and lasts for 36 days to cover the hurricane and ensuing restoration period.

165 **Table 1: Baseline and sensitivity runs used in this paper.**

Name	Description
Baseline	With forcing from atmosphere, rivers (from NWM) and precipitation, initialized with HYCOM GOFS 3.1
Baseline_Wave	Baseline with wave effects incorporated
No_NWM_precip	Baseline without rivers (via NWM) and precipitation
Ocean	Baseline forced by ocean and atmosphere only (but without precipitation)
NWM	Baseline forced by rivers only
Rain	Baseline forced by precipitation only

3.2 Coupling with NWM

River discharges are introduced into our model at its land boundary. First, ~6752 intersection points are identified between the NWM river segments and our land boundary (at 10m above sea level). The NWM flow time series
170 (https://water.noaa.gov/about/nwm) is then injected at the boundary elements immediately adjacent to those intersection points (Fig. 5), as sources (for inflow condition) or sinks (for outflow condition). The flow is then routed inside the SCHISM

domain by the model. The NWM segments that are explicitly incorporated into our grid during the mesh generation stage (Fig. 3c) facilitate the routing of water from watershed to coastal ocean. In addition, the rain that falls onto our grid domain is also routed together with the river flow. Note that the river flows injected at our model land boundary have indirectly

175   incorporated the precipitation that occurred *outside* (but not *inside*) the model domain, and therefore, the addition of direct precipitation onto our model domain is appropriate and is an integral component of the compound flood processes. To accurately simulate the initial movement of the very thin layer of rain water on the dry land, which is dominated by friction, a very small threshold of 10^{-6} m is used to differentiate between wet and dry states (Zhang et al., 2020). Since we have no information on the scalar concentrations for river inflows and rainfall, we applied 0 PSU for salinity and ambient water

180   temperature (i.e., the temperature at the local receiving cell calculated without accounting for the rivers or raindrops) for the injected river water and also for the rainfall. Obviously, the latter represents a source of uncertainty for the modelled temperature results. As explained in Huang et al. (submitted), heat exchange between air and water would misbehave on such a thin layer of water on watershed, so a threshold of 0.1 mm is set for local water depth, below which the heat exchange is turned off.

185   The assessment of NWM calculated flow against observed flow at the two largest rivers in the region is shown in Fig. 6. Similar to our findings for other storm events, this particular version of NWM produces flow that is generally consistent with USGS observation but tends to predict narrower and higher peaks, with roughly the same total volume of water during the event (Fig. 6). This forcing error should explain part of the model errors especially in the watershed. Note that the peak streamflow occurs about 4−6 days after the landfall, which is the time it takes for the rainfall induced flood to reach the

190   coastal rivers.

Natural Hazards
and Earth System
Sciences
Discussions

Open Access

EGU

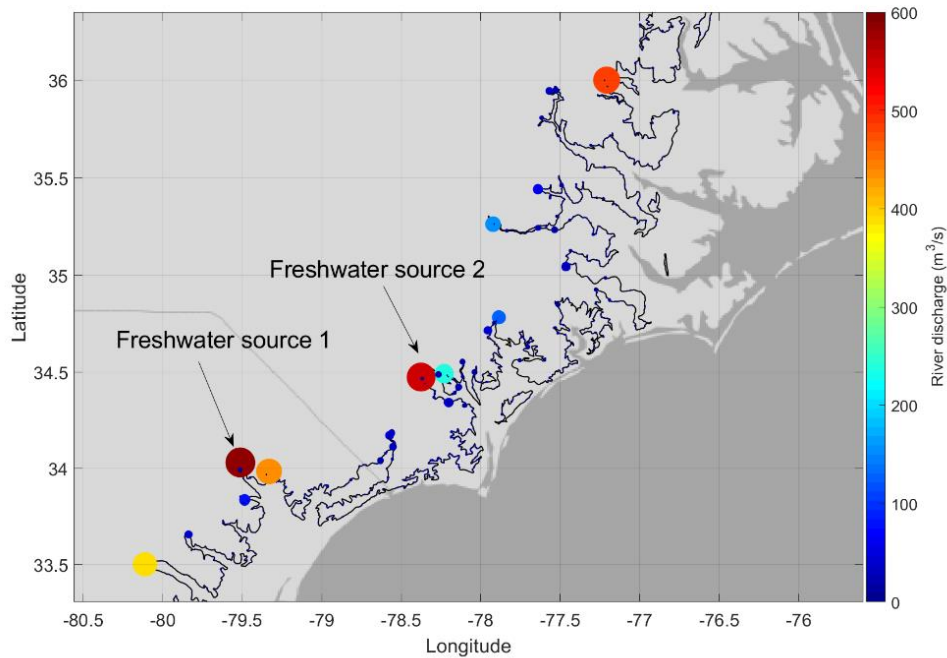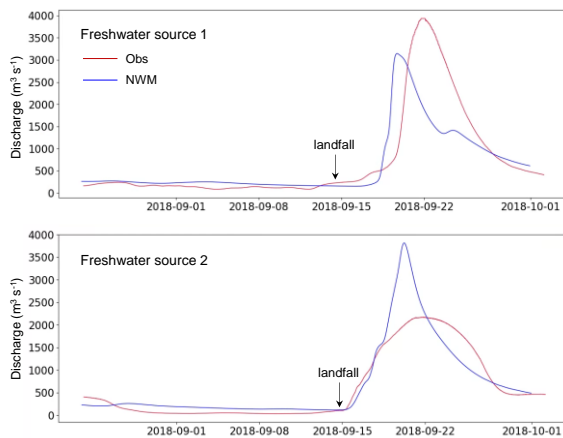**Fig. 5: Distribution of average river flow in North Carolina and South Carolina, from NWM.**

Fig. 6: Discharges at the two largest freshwater sources in the impact region (locations marked in Fig. 5). At each location, the NWM streamflow is taken at the intersection of the NWM segment and SCHISM's land boundary; the observation is based on the closest USGS station.
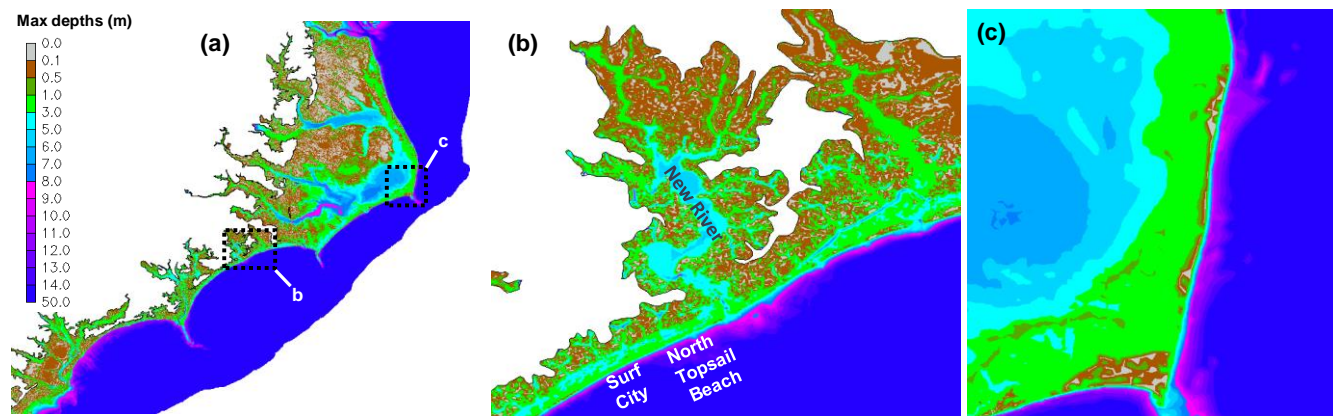
4 Model validation and sensitivity

200   In this section we will assess the model results for elevation, inundation and flow in the watershed and estuary. The spatial scales covered by the validation vary from O(10 km) to O(1 m). The model validation for non-storm period will not be discussed here; in short, the averaged amplitude error for the major constituent (M2 in east coast and K1 in northern Gulf of Mexico) for non-storm period is 3−4 cm (cf. Huang et al. submitted). We will start by looking at the wave effects nearshore.

4.1 Wave effects

205   Multiple breaches and over-toppings were reported across several NC barrier islands during the event, including Surf City, North Top Sail Beach, and New River inlet (https://www.wusa9.com/article/weather/before-and-after-hurricane-florence-changes-north-carolina-coastline/65-595918389). Some of these breaches may be related to significant wave activities; e.g. the maximum wave height at buoy 41025, ~30 km offshore from Cape Hatteras, reached ~10 m. Interestingly, the maximum wave heights are more modest nearer to the landfall: 4−6 m at Buoys 41159 and 41013 (see Fig. 3b for their locations).

210   Therefore, to investigate this possibility, we have also conducted a simulation with the wave model inside SCHISM activated ("Baseline_Wave" in Table 1). The details of the wave model (Wind Wave Model) have been described in Roland et al. (2012) and the coupled model has been applied to other systems (Guerin et al., 2018; Khan et al., 2020). The wave model was initialized and forced at the ocean boundary by a global Wave Watch III simulation (ftp://ftp.ifremer.fr/ifremer/ww3/HINDCAST), and used a spectral resolution of 36 directional bins and 24 frequency bins to

215   cover a frequency range of 0.04 to 1 Hz. The coupling time step between the two models (at which information was exchange including surface elevation, velocity and wave radiation stress) was 600 seconds.

    Our results indicate that the barrier islands near Surf City, North Top Sail Beach and New River inlet were indeed over-topped with 1−2 m of water (Fig. 7b; the locations of the islands can be seen in Fig. 8b). On the other hand, large portion of the island north of Cape Hatteras (Outer Banks) was spared (Fig. 7c), likely due to its N-S shoreline orientation, even with

220   the 10 m wave approximately 30 km offshore from there. More quantitative validation for the breaching processes is out of scope here because (1) we do not have accurate and update-to-date bathymetry just before the event, and (2) more importantly, a sediment transport study is required to simulate the bathymetric changes.

    The wave effects on the surface elevation are further quantified in Fig. 8, which suggests that the effects are most pronounced (with 30 cm or larger differences) inside the estuaries and Albemarle-Pamlico Sound (APS) due to large wave

225   breaking nearby. In the intermediate and deep water, however, the wave effects are on the order of a few centimetres and negligible (Fig. 8a). The Baseline results (without wave effects) also showed over-topping of the barrier islands similar to the Baseline_Wave (not shown).

Fig. 7: The maximum water depths from Baseline_Wave. The spatial extents of the local regions of (b) and (c) are marked in (a).
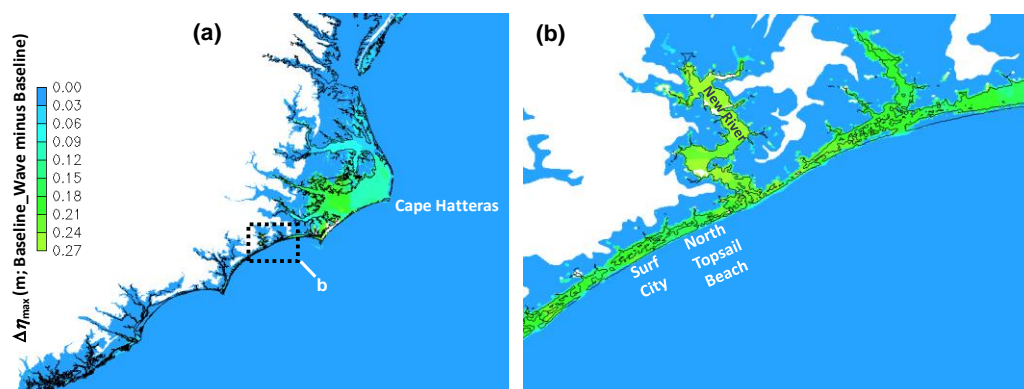

Fig. 8: Differences of the maximum elevations between Baseline_Wave and Baseline. (b) is zoom-in from (a). The thin black lines are the 0 m isobath.

In summary, the wave effects are significant nearshore and have contributed to the observed breaching and over-toppings of barrier islands. However, because the current study does not focus on the breaching processes and because of the significant computational overhead introduced by adding the wave model (>50%), we will proceed in the following by using the run without waves as the "baseline".

4.2 Bays and estuaries

We assess the calculated total water levels at 6 NOAA tide gauges near the impact area (cf. Fig. 3b). Three gauges are facing the open ocean (Charleston, Springmaid, and Wrightsville), and the other 3 gauges are either sheltered inside a bay (Beaufort) or behind barrier island (Hatteras and Oregon Inlet). The responses to the hurricane are different at those gauges. In particular, we see mostly set-downs at Charleston and Springmaid, surges of ~0.5 to 1 m at Wrightsville and Beaufort, and surges of ~30 cm followed by pronounced set-downs of ~40 cm at Hatteras and Oregon Inlet (Fig. 9). The different responses at these gauges are due to the wind curl of Florence that led to different dominant wind directions between

southern and northern stations, and are also due to specific geographic settings of each gauge. Most intriguing are the prominent set-downs observed at Hatteras and Oregon Inlet, which are explained by a combination of wind direction and blocking effects of barrier islands. Fig. 10 demonstrates that around the time of landfall of the hurricane, the predominantly westward wind felt in the Pamlico Sound has pushed water away from the barrier island. Meanwhile, the surge that

250 propagated from the ocean side is effectively blocked by the barrier island chain, thus creating a ~70 cm elevation difference between the waters immediately outside and inside the islands (Fig. 10), and the difference lasted for ~2 days (Fig. 9). The model captured the different regional responses quite well; overall, the averaged MAE (mean absolute error) for elevation is 11 cm. The addition of wave effects is seen to slightly increase the surge and rebounding waves at the last 3 gauges, resulting in slightly better model skills there.
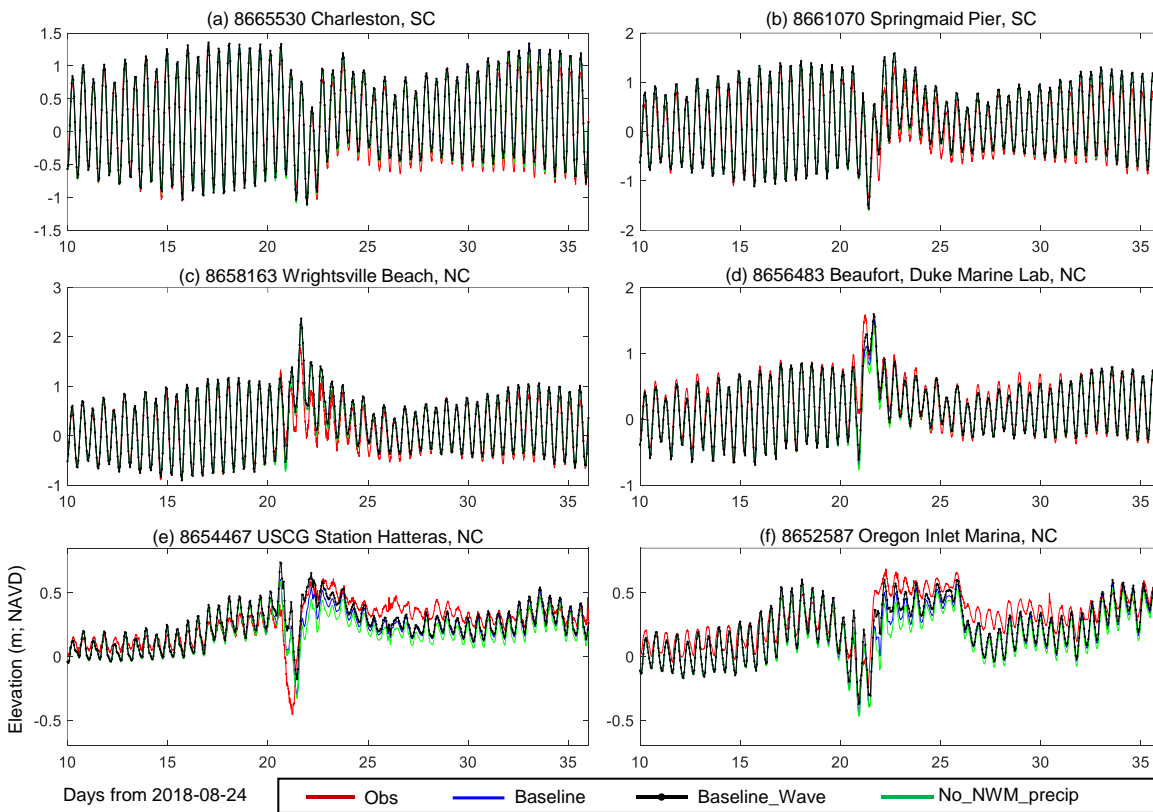
255

Fig. 9: Comparison of elevation at 6 NOAA gauges. Also included are results from 2 sensitivity runs (Baseline_Wave and No_NWM_precip; cf. Table 1). The two stations on the last row are on the back side of the barrier islands, thus showing larger differences between "baseline" and the sensitivity runs.
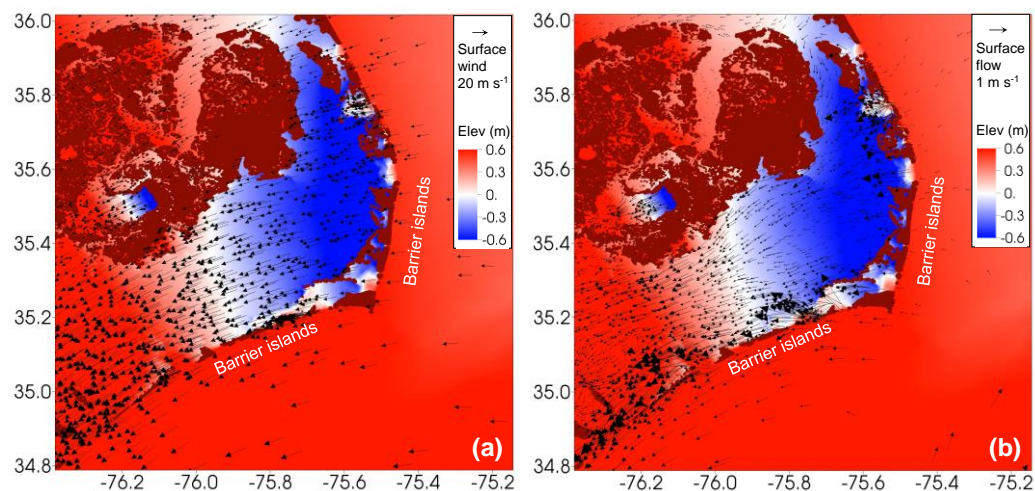
260

Fig. 10: Snapshots of water surface elevation at the time of Florence's landfall (2018-09-14) around the barrier islands near Cape Hatteras, overlaid by (a) wind speed and (b) water surface flow.

4.3 Watershed

High Water Marks (HWMs) are collected by USGS experts more than two weeks after Hurricane Florence's landfall on Sep. 14. They are derived from small seeds or floating debris carried by floodwaters that adhere to smooth surfaces or lodge in tree bark to form a distinct line, and also by stain lines on buildings, fences, and other structures. Therefore, HWMs are time sensitive and usually have vertical uncertainties of ± 0.3 feet (Koenig, et al., 2016; Austin, et al., 2018).

The simulated HWMs (276 of them) in the NC and SC watersheds are compared with field estimates (Fig. 11). The model is able to capture well the transition from estuarine to riverine regimes; note that the averaged bottom elevation for all observation points is 3.8 m based on NAVD88, and about 70% of the points are located above 2 m (NAVD88), beyond the reach of storm surges. Overall, the averaged MAE for all HWMs is 0.73 m, with a correlation coefficient of 0.92 and a positive mean bias of 0.09 m. These skill scores are similar to what we obtained for Hurricane Harvey (Huang et al. submitted) and are quite satisfactory given the large uncertainties typically found in the watersheds.
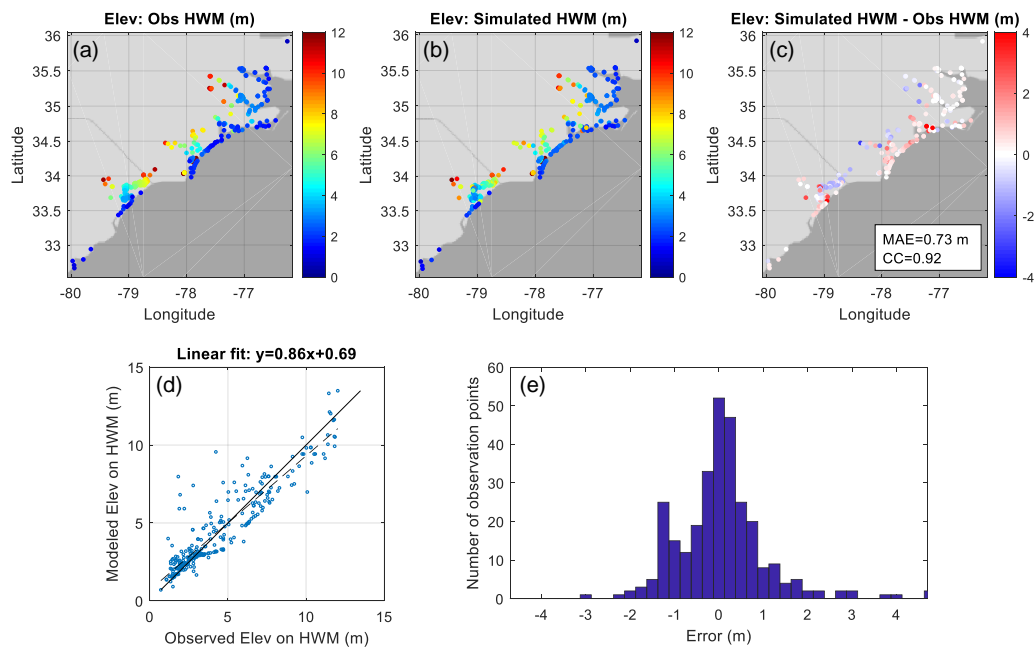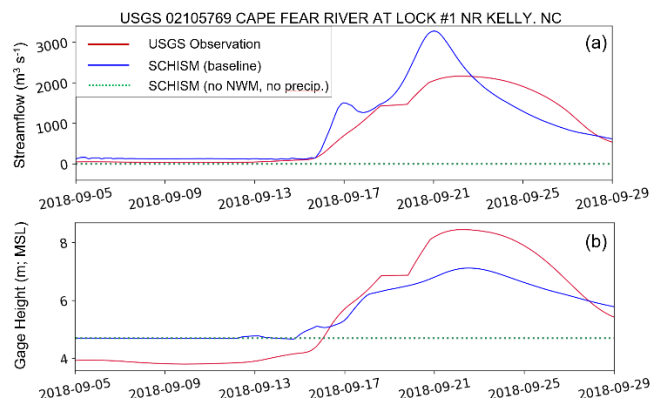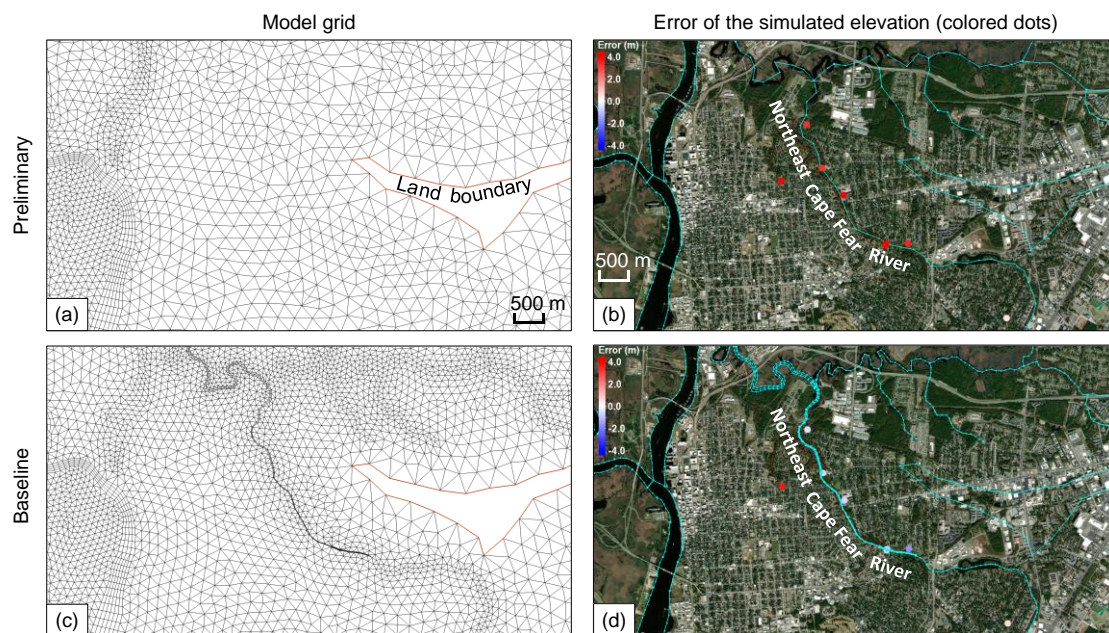
Fig. 11: Comparison of HWMs. (a) Field estimates from USGS; (b) model prediction; (c) model minus observation; (d) regression between model prediction and observation; (e) histogram showing the error distribution.

280   Some of the HWM estimates are derived from the measured time series at USGS in situ gauges. Fig. 12 shows the comparison in a large river in the region, at a gauge in the interior of our grid for both elevation (gauge height) and discharge. Because the observation's vertical datum is NAVD29 and the model's datum is NAVD88, we have adjusted the mean model elevations to match the observed mean in the elevation comparison (Fig. 12b); in other words, only the elevation variability is compared. Given all the uncertainties in the watershed, a reasonable agreement is found; our model

285   over-predicted the flow and under-predicted the flood-induced surges. Further calibration of the model, e.g. by adjusting the bottom friction should help improve the skill but given our ultimate goal of scaling up to the national scale in an operational setting, we chose to keep the parameterization as simple as possible here.

Fig. 12: Model−data comparison near the landfall location: (a) streamflow; (b) gauge height. The sensitivity run (without freshwater inputs from NWM or precipitation) is also shown, in which the channels are dry even during the hurricane, indicating they are beyond the storm surge influence. The station is away from the land boundary (location marked in Fig. 3b).

The model skill in the watershed was found to be sensitive to the grid resolution there, particularly in urban environment where small-scale structures (such as buildings and ditches) bring additional challenges and uncertainties (e.g., variable infiltration rates). Fig. 13 illustrates such an example around the Northeast Cape Fear River in the city of Wilmington, NC. Large HWM errors were found in the preliminary setup, because the computational grid did not resolve the small creeks that served as the main conduit in draining out the storm water after the flood. This resulted in stacking of water locally and thus large over-prediction of HWMs there. The channel of the creek is about 6–10 m wide, and once resolved using 2 rows of quads as done in the baseline (Fig. 13c), the model skill was greatly improved (Fig. 13d). The only remaining large error point in the "baseline" occurs in an urban area away from the river, likely due to the building effects that have not been incorporated in the model (Fig. 13d). Resolving small-scale flow routing features in a national scale requires automated tools such as Pysheds (https://github.com/mdbartos/pysheds) that can detect and delineate the channels automatically, which can then be effectively incorporated into grid generation tools such as SMS. Initial tests showed very promising results from this package. We remark that it is feasible to resolve these features efficiently without significantly increasing the grid size due to SCHISM's flexibility and robustness in handling poor-quality meshes.

16

Fig. 13: Importance of resolving small-scale features on the order of a few meters in the watershed, illustrated by a comparison
310 **between a preliminary setup (a, b) and the baseline setup (c, d). To better resolve the Northeast Cape Fear River, more SMS feature arcs (cyan lines in (d)) are used in the baseline setup than in the preliminary setup (cyan lines in (b)), significantly reducing the HWM errors. See Fig. 2 for the location of this locally zoomed-in region. The base maps in (b) and (d) are provided by ESRI.**

5 Compound effects

315   A carefully validated 3D model such as the one presented here can effectively separate out compounding factors from different sources: coastal surge, river flooding and precipitation. In this section we apply this approach to examine the contributing factors to the observed total flooding during Florence. The design of the numerical experiments is such that we selectively turn on/off forcing from ocean, river, and precipitation to examine their individual effects in isolation (Table 1). This section summarizes the major findings from those experiments.

320   Turning off both rivers and precipitation is expected to have major impact on flooding in the watershed. This is confirmed in Fig. 12 in the previous section. Not surprisingly, without rivers and precipitation, watershed is mostly dry as the storm surge cannot propagate over steep terrains (Fig. 12). As a result, the predicted HWMs are biased too low (Fig. 14) as the steep topography quickly damped out any surges brought in by the ocean. On the other hand, Zhang et al. (2020) demonstrated that the storm surges can propagate much further into watershed if watershed rivers are included.
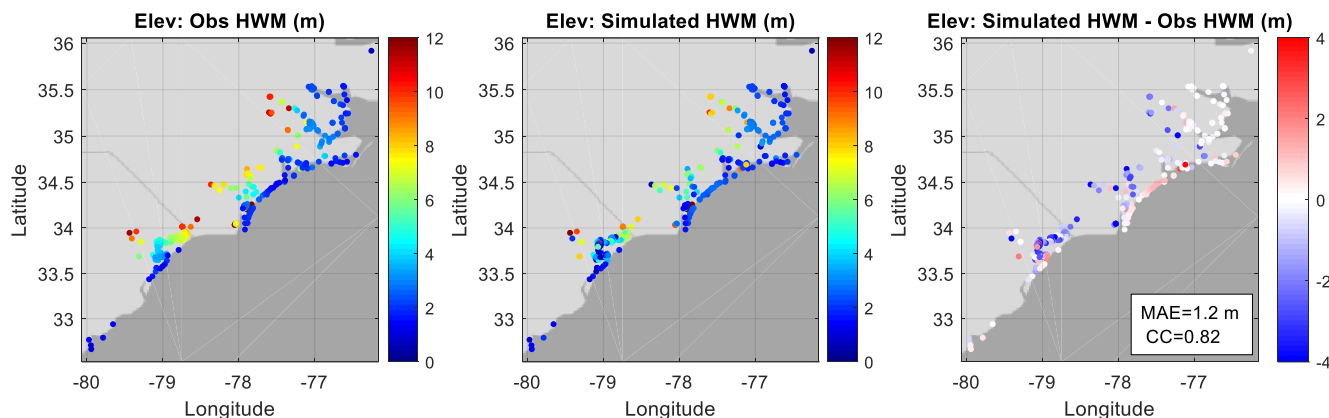
325

Fig. 14: Simulated HWMs from the sensitivity run "no_NWM_precip", i.e., without the freshwater inputs from NWM or precipitation. Note the underpredictions in the watershed and worse model skill compared with "baseline" (Fig. 11).

330   Less obvious are the effects of rivers and precipitation on the observed surges in the coastal bays. Fig. 9 indicates that the effects are negligible at the 3 coastal stations away from barrier islands (Fig. 9a−c), as the large amount of freshwater from the watershed directly drains into the coastal ocean (which has much larger volume of water). On the other hand, the impounding effects are clearly seen at the 2 stations behind the barrier islands (Fig. 9ef), where the discharged water is trapped for almost a week; the difference reaches ~30 cm at times there (cf. Fig. 8). As we showed in Section 4.2, the barrier

335   islands are effective in creating separation and thus large elevation gradient between water immediately outside and inside (cf. Fig. 10).

To assess the contributions from each of the 3 forcing factors to the total sum, we follow Huang et al. (submitted) and use the concept of "disturbance". We recognize that for compound flooding processes that involve both ocean and watershed, neither the water surface elevation nor the water depth is a satisfactory metric, because the nominally large water elevations

340   on the high ground of watershed are dominated by the high bottom elevation there, and the large water depths in the bays and ocean are dominated by the local bathymetry. Therefore, we adopt the concept of "disturbance", defined as:
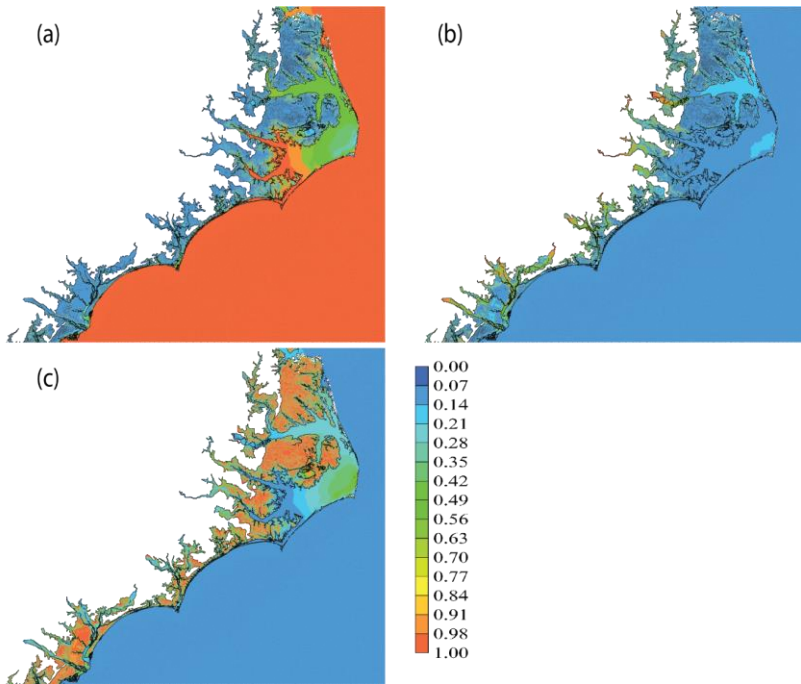
$$D = \begin{cases} \eta, & \text{if } h \geq 0, \\ \eta + h, & \text{if } h < 0, \end{cases}$$

where η is the water surface elevation and h is the bathymetry (positive downward; $h > 0$ for ocean and $h < 0$ for high grounds in watershed), so ($\eta + h$) is water depth. Basically, D represents the departure from "initial condition" (either the

345   initial water surface or bottom, whichever is higher). Note that D is continuous across $h = 0$. On the initially "dry" ground in watershed, D represents the local water depth; whereas at initially "wet" locations, D is simply the surface elevation. D is also a smoother metric to measure the compound effects as one transition from oceanic into watershed regimes.

18

The comparison between the maximum disturbances from the three experiments using only one of the three forcing factors and the total sum helps shed lights on the contributions from each. The results are presented in Fig. 15, in terms of

350 proportion of total maximum disturbance as explained by each forcing factor at a given location (therefore, the sum of all proportions equals unity). Our results clearly indicate that: (1) the ocean (and atmospheric) forcing dominates in the open and part of southern Pamlico Sound in the APS system; (2) river forcing is most dominant in the river network of watershed; (3) precipitation effects are dominant in other parts of the watershed away from the river network. However, the presence of the barrier islands significantly complicates the interaction among different forcings (e.g., the significant contribution from

355 precipitation in Pamlico Sound as shown in Fig. 15c). On the other hand, the inclusion of the wave effects is not expected to alter the findings here because their contribution to the total elevation is relatively minor as compared to the atmospheric effects (cf. Fig. 9).

The competition among different forcing factors in different regions can be succinctly summarized as a "dominance" map as shown in Fig. 16: a factor is deemed dominant if it explains at least 80% of the total disturbance; if, however, none of the

360 3 factors contribute to 80% or more at a particular place, the nonlinear compound effects are expected to be significant there. The ocean response is overwhelmingly dominated by the oceanic and atmospheric forcing, the response in the watershed rivers by the river flow, and the response in large portion of highly-elevated watersheds by the precipitation, as seen in Fig. 16. Most of the response in the southern Pamlico Sound is of oceanic origin, because of the wider openings to the south (Ocracoke and Hatteras inlets etc). On the other hand, there are only a few narrow inlets to the east (e.g. Oregon Inlet), thus

365 effectively blocking off the oceanic influence there (Fig. 16b; also cf. Fig. 10). It is the "grey areas" (Fig. 16) of compound flooding zones that are most intriguing. These include most of the APS and coastal rivers (Fig. 16b), where the weakened oceanic influence competes with river flow and large rainfall there (Fig. 15). In the estuaries with large river discharges with limited openings to the coastal ocean (Fig. 16c and Fig. 16e), the compound flooding zone is a result of competition among all 3 factors. On the other hand, for the estuaries to the south of the landfall in SC that are less influenced by the heavy

370 precipitation, and not protected by barrier islands and have smaller river discharges, oceanic effects can penetrate very deep into the coastal watershed (Fig.16d). The compound map like the one shown in Fig. 16 clearly demonstrates the urgent need for a holistic management approach in the planning of mitigation effort for the flood hazard during and after hurricane events.

Natural Hazards
and Earth System
Sciences
Discussions

Open Access

EGU

Fig. 15: Regional map showing portions explained by each forcing factor: (a) ocean force only ("Ocean" in Table 1); (b) river force only ("NWM" in Table 1); and (c) precipitation only ("Rain" in Table 1).
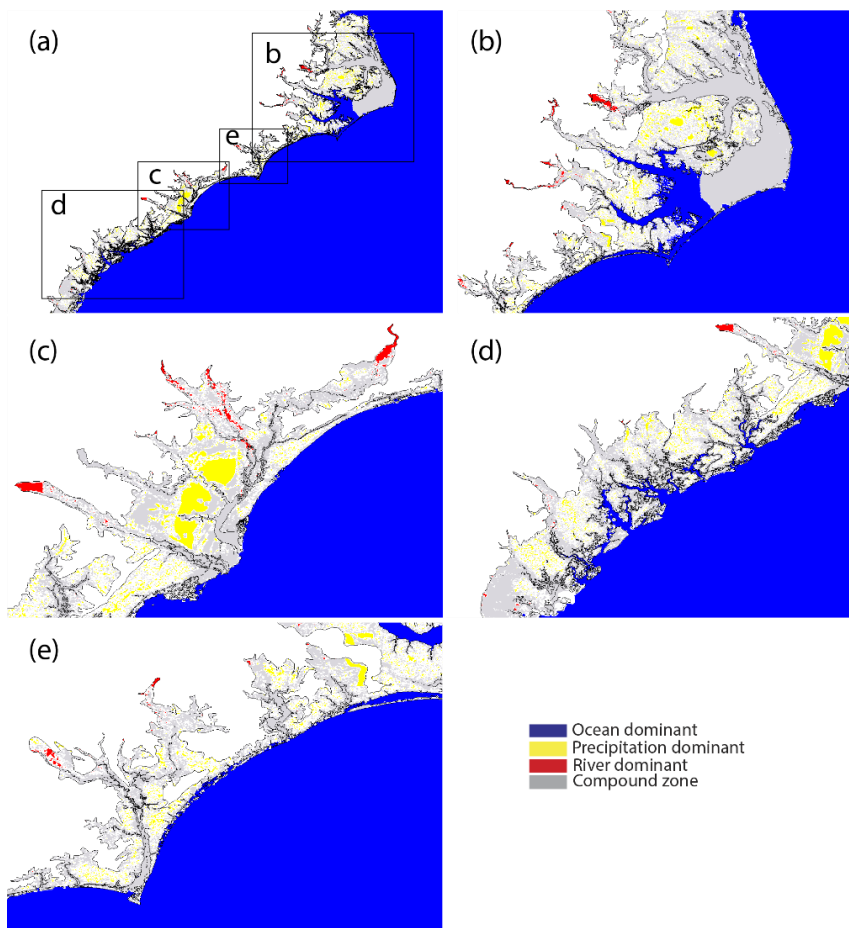
Fig. 16: Dominance map during Hurricane Florence. (b−e) are zoom-ins from (a) in different regions.

380

6 Conclusions

We have successfully applied a 3D cross-scale model to examine the compound flooding processes that occurred during Hurricane Florence. The model was validated with observation data collected in the watershed and coastal ocean. The mean absolute errors for major variables are: 11 cm for coastal elevation, 72 cm for High Water Marks (HWMs). Locally very

385 high resolution was used in some watershed areas to resolve small features that were critical for a good model skill for the HWMs. The wave effects were found to be significant near barrier islands and had contributed to some over-toppings and breaches there. The validated model was then used to reveal significant nonlinear compound effects in most parts of coastal watersheds and behind the barrier islands. The barrier islands were shown to be particularly effective in separating the processes in the water bodies inside and outside.

390 The results of the current study, especially the regional compound zone map, filled in a critical knowledge gap in our understanding of compound flooding events. In fact, operational forecasts based on the current model are being set up at

NOAA to help coastal resource and emergency managers with disaster planning and mitigation effort. The model can also be used to facilitate new scientific discovery of novel coastal processes; for example, preliminary results for the fate of pollutants discharged from the watershed suggest that the large watershed outflow resulted from heavy precipitation played

395 an essential role in exporting pollutants far into the ocean through the large and long-lasting freshwater plumes that occurred after the event.

Data availability

The model source code is freely available at https://github.com/schism-dev.

400 **Author contributions**

All authors conceived the idea of the study under the NOAA's Water Initiative project; FY, WH and YJZ developed the methodology with the support of other co-authors; FY and WH produced the results with the support of YJZ, HY; FY analyzed the results with the support of other co-authors. All authors contributed to writing of the paper.

Competing interests.

405 The authors declare that they have no conflict of interest.

Acknowledgements

415 **References**

Austin, S.H., Watson, K.M., Lotspeich, R.R., Cauller, S.J., White, J.S., and Wicklein, S.M.: Characteristics of peak streamflows and extent of inundation in areas of West Virginia and southwestern Virginia affected by flooding, June 2016 (ver. 1.1, September 2018): U.S. Geological Survey Open-File Report 2017–1140, 35 p., https://doi. org/10.3133/ofr20171140, 2018.

420 Cai, X., Zhang, Y.J., Shen, J., Wang, H., Wang, Z., Qin, Q. and Ye, F.: A Numerical Study of Hypoxia in Chesapeake Bay Using an Unstructured Grid Model: Validation and Sensitivity to Bathymetry Representation. Journal of the American Water Resources Association, https://doi.org/10.1111/1752-1688.12887, 2020.

Natural Hazards
and Earth System
Sciences
Discussions

EGU

Open Access

Ezer, T.: On the interaction between a hurricane, the Gulf stream and coastal sea level. Ocean Dyn. 68 (10), 1259–1272, 2018.

425 Chen, W.B. and Liu, W.C.:. Modeling flood inundation induced by river flow and storm surges over a river basin. Water, 6(10), pp.3182-3199, 2014.

Chen, A.S., Djordjević, S., Leandro, J. and Savić, D.A.: An analysis of the combined consequences of pluvial and fluvial flooding. Water Science and Technology, 62(7), pp.1491-1498, 2020.

Cho, K.H., Wang, H.V., Shen, J., Valle-Levinson, A. and Teng, Y.C.: A modeling study on the response of Chesapeake Bay

430 to hurricane events of Floyd and Isabel. Ocean Modelling, 49, pp.22-46, 2012.

Feaster T.D., Weaver J.C., Gotvald A.J., Kolb K.R.: Preliminary peak stage and streamflow data for selected US Geological Survey streamgaging stations in North and South Carolina for flooding following Hurricane Florence, September 2018. US Geological Survey, 2018.

Dresback, K.M., Fleming, J.G., Blanton, B.O., Kaiser, C., Gourley, J.J., Tromble, E.M., Luettich Jr, R.A., Kolar, R.L., Hong,

435 Y., Van Cooten, S. and Vergara, H.J.: Skill assessment of a real-time forecast system utilizing a coupled hydrologic and coastal hydrodynamic model during Hurricane Irene (2011). Continental Shelf Research, 71, pp.78-94, 2013.

Guérin, T., Bertin, X., Coulombier, T., de Bakker, A.: Impacts of wave-induced circulation in the surf zone on wave setup. Ocean Model. 123, 86–97, 2018.

Hall, T.M. and Kossin, J.P.: Hurricane stalling along the North American coast and implications for rainfall. Clim. Atmos.

440 Sci. 2, 17, doi:10.1038/s41612-019-0074-8ence, 2019.

Huang, W., Ye, F., Zhang, Y., Park, K., Du, J., Moghimi, S., Myers, E., Pe'eri, S., Calzada, J.R., Yu, H.C., Nunez, K., and Liu, Z.: Compounding factors for extreme flooding around Galveston Bay during Hurricane Harvey, Ocean Modelling, submitted, 2020.

Ikeuchi, H., Hirabayashi, Y., Yamazaki, D., Muis, S., Ward, P.J., Winsemius, H.C., Verlaan, M. and Kanae, S.: Compound

445 simulation of fluvial floods and storm surges in a global coupled river-coast flood model: Model development and its application to 2007 Cyclone Sidr in Bangladesh. Journal of Advances in Modeling Earth Systems, 9(4), pp.1847-1862, 2017.

Khan, J., Durand, F., Testut, L., Krien, Y., Islam, A.K.M.: Sea level rise inducing tidal modulation along the coasts of Bengal delta, Continental Shelf Research, 211, https://doi.org/10.1016/j.csr.2020.104289, 2020.

450 Koenig, T.A., Bruce, J.L., O'Connor, J.E., McGee, B.D., Holmes, R.R., Jr., Hollins, Ryan, Forbes, B.T., Kohn, M.S., Schellekens, M.F., Martin, Z.W., and Peppler, M.C.: Identifying and preserving high-water mark data: U.S. Geological Survey Techniques and Methods, book 3, chap. A24, 47 p., http://dx.doi.org/10.3133/tm3A24, 2016.

Kumbier, K., Carvalho, R. C., Vafeidis, A. T. & Woodroffe, C. D.: Investigating compound flooding in an estuary using hydrodynamic modelling: A case study from the Shoalhaven River, Australia. Natural Hazards and Earth System Sciences, 455 18 (2), 463-477, 2018.

Muñoz, D.F., Moftakhari, H. and Moradkhani, H.: Compound effects of flood drivers and wetland elevation correction on coastal flood hazard assessment. Water Resources Research, 56(7), p.e2020WR027544, 2020.

Pasquier, U., He, Y., Hooton, S., Goulden, M. and Hiscock, K.M.: An integrated 1D–2D hydraulic modelling approach to assess the sensitivity of a coastal region to compound flooding hazard under climate change. Natural Hazards, 98(3), pp.915-460 937, 2019.

Pfahl, S., O'Gorman, P.A., and Fischer, E.M.: Understanding the regional pattern of projected future changes in extreme precipitation. Nat. Clim. Chang. 7, 423-427, 2017.

Roland, A., Zhang, Y., Wang, H.V., Meng, Y., Teng, Y., Maderich, V., Brovchenko, I., Dutour-Sikiric, M. and Zanke, U.: A fully coupled wave-current model on unstructured grids, Journal of Geophysical Research-465 Oceans,117,C00J33,doi:10.1029/2012JC007952, 2012.

Santiago-Collazo, F.L., Bilskie, M.V., Hagen, S.C.: A comprehensive review of compound inundation models in low-gradient coastal watersheds. Environ. Model. Software 119:166–181. https://doi.org/10.1016/j.envsoft.2019.06.002, 2019.

Umlauf, L. and Burchard, H.: A generic length-scale equation for geophysical turbulence models. J. Mar. Res., 61, 235-265, 2003.

Wing, O.E., Sampson, C.C., Bates, P.D., Quinn, N., Smith, A.M. and Neal, J.C.: A flood inundation forecast of Hurricane 470 Harvey using a continental-scale 2D hydrodynamic model. Journal of Hydrology X, 4, p.100039, 2019

Ye, F., Zhang, Y.J., Wang, H.V., Friedrichs, M.A., Irby, I.D., Alteljevich, E., Valle- Levinson, A., Wang, Z., Huang, H., Shen, J., Du, J.: A 3D unstructured-grid model for Chesapeake Bay: Importance of bathymetry. Ocean Model. 127, 16–39, 2018.

Ye, F, Zhang. Y., Yu, H., Sun, W., Moghimi, S, Myers, E.P., Nunez, K., Zhang, R., Wang, H.V., Roland, A., Martins, K., 475 Bertin, X., Du, J., Liu, Z.: Simulating storm surge and compound flooding events with a creek-to-ocean model: importance of baroclinic effects. Ocean Model 145, 101526. https://doi.org/10.1016/j.ocemod.2019.101526, 2020.

Zhang, Y., Ateljevich, E., Yu, H.-C., Wu, C.H., and Yu, J.C.S.: A new vertical coordinate system for a 3D unstructured-grid model. Ocean Modelling, 85, 16-31., 2015.

Zhang, Y., Ye, F., Stanev, E.V., Grashorn, S.: Seamless cross-scale modeling with SCHISM. Ocean Model 102:64–81, 480 2016.

Zhang, Y., Ye, F., Yu, H., Sun, W., Moghimi, S., Myers, E., Nunez, K., Zhang, R., Wang, H., Roland, A., Du, J., Liu, Z.: Simulating compound flooding events in a hurricane. Ocean Dyn. 70, 621–640, 2020.

24